Topology-cognizant Optimal Power Flow in Multi-terminal DC Grids

Tuncay Altun, *Student Member, IEEE,* Ramtin Madani, *Member, IEEE,* and Ali Davoudi, *Senior Member, IEEE*

***Abstract*—In this paper, we propose a topology-cognizant optimal power flow (OPF) paradigm with additional safety constraints for multi-terminal direct current (MTDC) grids. The resulting formulation is concerned with the optimization of controller set-points, i.e., voltage and power levels at each bus, and the switching status of transmission lines that collectively referred to as grid topology. A pair of additional safety constraints are integrated into the problem formulation to prevent voltage violations caused by power fluctuations in between two controller set-point updates. Searching for a grid topology that offers more efficient operation leads to a mixed-integer nonlinear program (MINLP) which is computationally challenging due to: i) Non-convex power flow equations, (ii) Non-convex converter loss equations, and iii) Binary variables accounting for the operational status of transmission lines. Non-convexities of power flows and converter loss equations are tackled by means of a mixed-integer second-order cone programming (MISOCP) relaxation, while the optimal switching status of transmission lines are determined via a branch-and-bound search. Numerical results for the modified IEEE 14, 30, and 57-bus systems are used to verify the merits of the proposed method. Furthermore, this method is experimentally validated using the CIGRE B4 DC grid benchmark in a real-time hardware-in-the-loop platform.**

***Index Terms*—HVDC transmission, multi-terminal dc grids, optimal power flow, optimal transmission switching.**

I. Introduction

Multi-terminal direct current (MTDC) grids are becoming popular due to superior efficiency. Additionally, they are suitable candidates for offshore wind farms integration [1] or long-distance power exchange (e.g., European supergrid [2]) because of simpler control mechanism without challenges native to AC grids. Moreover, voltage-source converters (VSCs) based MTDC grids allow interconnection with weak AC grids, black start in the case of blackouts, and power flow reversal without switching the voltage polarity [3]. Given their superiority over AC power transmission, there are ongoing efforts to realize bulk power exchange among independent grids using the VSC technology. VSC's DC voltage control is the key measure to proper power dispatch and loss management in a MTDC grid, and is mainly done via master-slave [4], voltage margin [5], or voltage droop [6] mechanisms. Droop control approach is more dependable than voltage margin and master-slave controls if several converters actively participate in the regulation process [7].

The two-tier control hierarchy of MTDC grids [8], [9] includes a faster, lower-level droop controller that locally regulates the VSC voltage at the cost of power sharing objectives. Hence, the upper-level optimizer periodically tunes the set-points of the lower-level droop control to meet predefined optimization objectives, i.e, minimizing generation cost, transmission loss, etc. The optimization involved in tuning droop set-points could become computationally prohibitive for real-time applications [10]. This delay, or any interruption in the communication between the two control layers, could cause a prescribed droop set-point to violate an operational safety limit, particularly if the load demand or power generation fluctuate noticeably before the subsequent droop set-points update [11], [12]. Preventive measures, while still pursuing optimality in MTDC grids, are rare in the literature, e.g., see [13]–[15]. Hence, the development of a reliable preventive strategy is one of the primary motivations of the present work.

The optimal power flow (OPF) in MTDC grids aims to minimize transmission loss alone [16] or along with conversion loss [17]. Convex relaxation methods can transform nonlinear power flow optimization into convex surrogates by reformulating it in a high-dimensional space while preserving the equivalency with the original non-convex problem [18], [19]. These approaches have been extended to the static OPF problem of MTDC grids that also suffer from non-convex converter loss equations [20]–[22].

Static OPF solutions, however, overlook the optimal switching of transmission lines that can help reduce the total generation cost [23]–[26], line overloads [27]–[29], and transmission losses [30]–[32], as well as help address voltage violations [33]–[35], protect the grid from abnormal operations [36], [37], prevent the load shed caused by contingency events [38], or schedule maintenance [39]. A transmission line built for a long-term requirement could exhibit dispatch inefficiencies [40]. From an optimization perspective, determining the statuses of transmission lines could result in a mixed-integer nonlinear programming (MINLP) problem that can be computationally challenging [32]. Heuristic methods, such as successive branch reduction approach [32], particle swarm optimization [34], [37], or genetic [23], artificial immune [28], and firefly-evolutionary [36] algorithms have been used to solve this problem. Besides heuristic methods, many deterministic, i.e., mathematical programming, approaches are employed to generate feasible solutions. [24]–[26] approximate the original MINLP formulation as a mixed-integer linear programming (MILP) that, in some cases, could result in voltage collapse as physical laws are not properly respected, i.e, network losses are neglected [33]. To integrate network losses into the problem formulation, [30] and [33] present a two-stage optimization model, where MILP version of the

T. Altun was with the University of Texas at Arlington, USA. He will be with the Yozgat Bozok University, Yozgat, Turkey. R. Madani and A. Davoudi are with the University of Texas at Arlington, USA. This work is supported by the National Science Foundation under award ECCS-1809454.

problem is handled as a *master problem*, while the MINLP problem is addressed as a *subproblem*. Albeit [30] and [33] tackle the MINLP problem formulation, their solutions are not guaranteed to be globally optimal.

An AC grid topology optimization problem, with exact loss modeling, was first introduced in [31] as a mixed-integer cone programming formulation. For that, a globally optimal solution, up to a desired accuracy, can be found using available commercial solvers. Recently, various convex relaxation methods, including mixed-integer semi-definite programming [35] and mixed-integer second-order cone programming (MISOCP) [41]–[43] have been applied for solving AC grid topology optimization problems. The authors have developed a MISOCP model to reconfigure a DC network to minimize the generational cost in static OPF and secure the operation in response to contingencies [44]. MTDC grid, unlike DC or AC networks, includes operation in high voltage, presence of VSCs, and combination of AC and DC grid constraints that bring additional complexities into its MISOCP formulation. Accordingly, this paper offers a MISOCP formulation for the topology-cognizant OPF in MTDC grids to minimize both transmission and converter losses while respecting physical and operational constraints including AC part and VSC characteristics. The proposed formulation involves safety constraints that prevent voltage violations caused by power fluctuation in between two droop set-point updates. The noticeable contributions of this paper are summarized as:

- Static OPF is extended to obtain a topology-cognizant OPF model with binary variables accounting for the switching status of transmission lines.
- The proposed MINLP model is transformed into a MISOCP surrogate to obtain a tractable topology-cognizant OPF formulation for MTDC grids.
- Additional constraints, that sustain a safe operation by further restricting voltage limits in response to volatile generation/load profiles in between two droop set-point updates, are integrated into the problem formulation.
- A penalty function is incorporated into problem formulation to address instances when the topology-cognizant OPF problem fails to produce a feasible solution.

The rest of the paper has the following organization. Section II contains preliminary materials. Section III elaborates the modeling of MTDC grids. Section IV incorporates the switching actions of transmission lines into the OPF problem, and presents its convexified version. In Section V, the OPF and topology-cognizant OPF solutions are experimentally and numerically validated through CIGRE B4 DC grid benchmark and several modified IEEE benchmarks, respectively.

II. Notations and Grid Terminologies

A. Notations

Bold small letter, $(\boldsymbol{x})$, and capital letter, $(\boldsymbol{X})$, represent vectors and matrices, respectively. $\mathbf{1}$ and $\mathbf{0}$ refer to vectors with all elements as 1 and 0, respectively. The sets of complex and real numbers are symbolized with $\mathbb{C}$ and $\mathbb{R}$ respectively. $\mathbb{H}^n$ and $\mathbb{S}^n$ represent the hermitian and symmetric matrices size of $n \times n$, respectively. $\mathrm{imag}\{\cdot\}$ and $\mathrm{real}\{\cdot\}$ define the imaginary and real parts of a complex number or matrix, respectively. A matrix's i^{th} row and j^{th} column is referred with (i, j). The transpose and conjugate transpose operators are denoted with $(\cdot)^\top$ and $(\cdot)^*$, respectively. $|\cdot|$ refers the cardinality of a set or the absolute/magnitude value of a vector/scalar. $\mathrm{tr}\{\cdot\}$ refers to the trace of a given matrix. $\|\cdot\|_2$ stands for the euclidean norm of a vector. $\mathrm{diag}\{\cdot\}$ creates a vector using the matrix's diagonal entries. $[\cdot]$ composes a matrix with diagonal entries from a given vector.

B. Grid Terminologies

Figure 1 demonstrates a schematic for an MTDC grid. Grid buses are connected via DC transmission lines. Terminologies for grid elements are elaborated here:

- **DC Grid:** The DC transmission grid is structured using directed graph $\mathcal{H} = (\mathcal{N}, \mathcal{L})$ where the sets of buses and lines are denoted by $\mathcal{N}$ and $\mathcal{L}$, respectively. The DC grid *from* and *to* line-incidence matrices are defined with the pairs $\vec{\boldsymbol{L}}, \overleftarrow{\boldsymbol{L}} \in \{0,1\}^{|\mathcal{L}|\times|\mathcal{N}|}$, respectively. $\vec{L}_{lk} = 1$ ($\overleftarrow{L}_{lk} = 1$) for every $k \in \mathcal{N}$ and $l \in \mathcal{L}$, if and only if the transmission line l starts(ends) at bus, k. The matrices $\boldsymbol{Y} \in \mathbb{R}^{|\mathcal{N}|\times|\mathcal{N}|}$, $\vec{\boldsymbol{Y}}, \overleftarrow{\boldsymbol{Y}} \in \mathbb{R}^{|\mathcal{L}|\times|\mathcal{N}|}$ represent the bus-conductance, and the *from* and *to* line-conductance matrices of the DC grid, respectively. The *from* and *to* vectors of transmission line power flows are defined as $\vec{\boldsymbol{f}}$ and $\overleftarrow{\boldsymbol{f}} \in \mathbb{R}^{|\mathcal{L}|}$, respectively. The power flow limits is represented with $\vec{\boldsymbol{f}}^{\max} \in (\mathbb{R} \cup \{\infty\})^{|\mathcal{L}|}$. Additionally, $\vec{\boldsymbol{x}} \in \{0,1\}^{|\mathcal{L}|}$ defines the vector that acts for the switching status of transmission lines. Let $\vec{\boldsymbol{x}}_{\min}, \vec{\boldsymbol{x}}_{\max} \in \{0,1\}^{|\mathcal{L}|}$ encapsulate prior knowledge of the on/off switches, i.e.,

$$\begin{aligned}
&\vec{x}_{\min_l} = \vec{x}_{\max_l} = 0, && \text{if line } l \in \mathcal{L} \text{ is known to be disconnected,}\\
&\vec{x}_{\min_l} = \vec{x}_{\max_l} = 1, && \text{if line } l \in \mathcal{L} \text{ is known to be connected,}\\
&\vec{x}_{\min_l} = 0, \quad \vec{x}_{\max_l} = 1, && \text{otherwise.}
\end{aligned}$$

  Finally, let $\boldsymbol{v}^{\mathrm{dc}}, \boldsymbol{p}^{\mathrm{dc}} \in \mathbb{R}^{|\mathcal{N}|}$ represent the vectors of DC bus voltages and active power injections into the DC side.
- **Buses/VSCs:** Each DC bus $k \in \mathcal{N}$ is assumed to accommodate a single voltage-source converter (VSC) which is connected to a set of loads and generators through a phase reactor, modeled as a series impedance $z_k \in \mathbb{C}$. Define $\boldsymbol{z}, \boldsymbol{i}^{\mathrm{ac}} \in \mathbb{C}^{|\mathcal{N}|}$ as the vectors of phase-reactor impedance and current values, respectively. Let $\boldsymbol{v}_{\mathrm{c}}^{\mathrm{ac}}, \boldsymbol{v}_{\mathrm{f}}^{\mathrm{ac}} \in \mathbb{C}^{|\mathcal{N}|}$ account for the vectors of VSC and load/generation-side AC voltages, respectively. Let $\boldsymbol{s}^{\mathrm{ac}} \in \mathbb{C}^{|\mathcal{N}|}$, and $\boldsymbol{p}^{\mathrm{ac}}, \boldsymbol{q}^{\mathrm{ac}} \in \mathbb{R}^{|\mathcal{N}|}$, respectively, represent the vectors of apparent, active and reactive power injections from VSCs into the AC sides.
- **Generators/Loads:** Let $\mathcal{G}$ be the set for generators and $\boldsymbol{G} \in \{0,1\}^{|\mathcal{G}|\times|\mathcal{N}|}$ as the generator incidence matrix, where $G_{gk} = 1$ if and only if the generator $g \in \mathcal{G}$ is located at the AC side of the bus $k \in \mathcal{N}$. $\boldsymbol{s}^{\mathrm{g}} \in \mathbb{C}^{|\mathcal{G}|}$ and $\boldsymbol{p}^{\mathrm{g}}, \boldsymbol{q}^{\mathrm{g}} \in \mathbb{R}^{|\mathcal{G}|}$, respectively, represent the vectors of apparent, active and reactive power generations. Define $\mathcal{D}$ as the set of loads and $\boldsymbol{D} \in \{0,1\}^{|\mathcal{D}|\times|\mathcal{N}|}$ as the load incidence matrix where $D_{dk} = 1$ if and only if the load

This article has been accepted for publication in a future issue of this journal, but has not been fully edited. Content may change prior to final publication. Citation information: DOI 10.1109/TPWRS.2021.3067025, IEEE Transactions on Power Systems

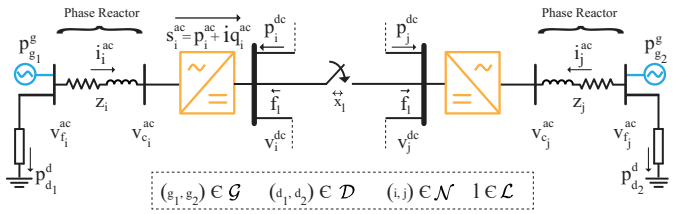

Fig. 1. A portion of a meshed MTDC grid. The grid is equipped with switching devices to enable line switching decisions, $\bar{x}$. VSCs couple AC and DC parts by controlling their voltage and power levels on both sides.

$d \in \mathcal{D}$ is located at the AC side of the bus $k \in \mathcal{N}$. Finally, $\boldsymbol{p}^{\mathrm{d}} \in \mathbb{R}^{|\mathcal{D}|}$ represents the vectors of active power demand.

III. MTDC Grid Model

A. AC/DC Coupling

VSC losses are approximated by a quadratic polynomial with respect to current magnitude as

$$\boldsymbol{p}^{\mathrm{conv}}_{\mathrm{loss}} \triangleq -\boldsymbol{p}^{\mathrm{ac}} - \boldsymbol{p}^{\mathrm{dc}} = \boldsymbol{a} + [\boldsymbol{b}]|\boldsymbol{i}^{\mathrm{ac}}| + [\boldsymbol{c}]|\boldsymbol{i}^{\mathrm{ac}}|^2, \tag{1}$$

where $\boldsymbol{a}, \boldsymbol{b}, \boldsymbol{c} \in \mathbb{R}^{|\mathcal{N}|}$ are the vectors of positive coefficients [20], and $\boldsymbol{p}^{\mathrm{ac}}$ and $\boldsymbol{p}^{\mathrm{dc}}$ are the vectors of active power injections by the VSCs into the AC and DC sides, respectively. Additionally, the AC and DC side voltages are related with a modulation factor, m,

$$|\boldsymbol{v}^{\mathrm{ac}}_{\mathrm{c}}| \leq \sqrt{\frac{3}{2}} m \boldsymbol{v}^{\mathrm{dc}}. \tag{2}$$

B. VSC Limits

The AC side complex powers can be calculated as

$$\boldsymbol{s}^{\mathrm{ac}} = [\boldsymbol{v}^{\mathrm{ac}}_{\mathrm{c}}] \left([\boldsymbol{z}]^{-1}(\boldsymbol{v}^{\mathrm{ac}}_{\mathrm{c}} - \boldsymbol{v}^{\mathrm{ac}}_{\mathrm{f}})\right)^*, \tag{3}$$

with the VSCs active power is bounded as

$$\boldsymbol{p}^{\mathrm{ac}}_{\min} \leq \boldsymbol{p}^{\mathrm{ac}} \leq \boldsymbol{p}^{\mathrm{ac}}_{\max}. \tag{4}$$

With no loss of generality, the VSC reactive power limits can be formulated as

$$-m_{\mathrm{b}}|\bar{\boldsymbol{s}}^{\mathrm{ac}}| \leq \boldsymbol{q}^{\mathrm{ac}} \leq [|\mathrm{imag}\{\boldsymbol{z}\}|]^{-1}\left[\boldsymbol{v}^{\mathrm{ac}}_{\mathrm{c}_{\max}}\right](\boldsymbol{v}^{\mathrm{ac}}_{\mathrm{c}_{\max}} - |\boldsymbol{v}^{\mathrm{ac}}_{\mathrm{f}}|), \tag{5}$$

where m_{b} is a positive constant, and $|\bar{\boldsymbol{s}}^{\mathrm{ac}}|$ is the vector of nominal VSC apparent power values [17]. The right side of inequality (5) is the outcome of the approximation on phase-angle difference between phase reactor buses, $\theta_{c_i} - \theta_{f_i} = 0$ for every $i \in \mathcal{N}$. To further simplify (5) while finding the maximum reactive power constraint, one can substitute $|\boldsymbol{v}^{\mathrm{ac}}_{\mathrm{f}}|$ with$\boldsymbol{v}^{\mathrm{ac}}_{\mathrm{f}_{\min}}$ [20]. Finally, according to Ohm's law,

$$\boldsymbol{i}^{\mathrm{ac}} = [\boldsymbol{z}]^{-1}(\boldsymbol{v}^{\mathrm{ac}}_{\mathrm{c}} - \boldsymbol{v}^{\mathrm{ac}}_{\mathrm{f}}), \tag{6}$$

and the current magnitude $|\boldsymbol{i}^{\mathrm{ac}}|$, should not exceed an upper limit $|\boldsymbol{i}^{\mathrm{ac}}_{\max}|$, to be compatible with the limits of phase reactor and controller.

C. Generator/Load Limits

Active power balance at the generator/load sides of phase reactors can be formulated as

$$\boldsymbol{G}^\top \boldsymbol{p}^{\mathrm{g}} - \boldsymbol{D}^\top \boldsymbol{p}^{\mathrm{d}} = \mathrm{real}\{[\boldsymbol{v}^{\mathrm{ac}}_{\mathrm{f}}]\left([\boldsymbol{z}]^{-1}(\boldsymbol{v}^{\mathrm{ac}}_{\mathrm{f}} - \boldsymbol{v}^{\mathrm{ac}}_{\mathrm{c}})\right)^*\}, \tag{7}$$

with

$$\boldsymbol{p}^{\mathrm{g}}_{\min} \leq \boldsymbol{p}^{\mathrm{g}} \leq \boldsymbol{p}^{\mathrm{g}}_{\max}, \tag{8}$$

$$\boldsymbol{v}^{\mathrm{ac}}_{\mathrm{f}_{\min}} \leq |\boldsymbol{v}^{\mathrm{ac}}_{\mathrm{f}}| \leq \boldsymbol{v}^{\mathrm{ac}}_{\mathrm{f}_{\max}}, \tag{9}$$

enforcing generator/load power and voltage limits.

D. DC Grid Constraints

Nodal power balance equations of the DC grid can be formulated as

$$\vec{\boldsymbol{L}}^\top \vec{\boldsymbol{f}} + \overleftarrow{\boldsymbol{L}}^\top \overleftarrow{\boldsymbol{f}} = \boldsymbol{p}^{\mathrm{dc}}, \tag{10}$$

where $\vec{\boldsymbol{f}}$ and $\overleftarrow{\boldsymbol{f}}$ are dictated by nodal DC voltages and the status of transmission lines:

$$\vec{\boldsymbol{f}} = [\vec{\bar{\boldsymbol{x}}}]\,\mathrm{diag}\{\vec{\boldsymbol{L}}\boldsymbol{v}^{\mathrm{dc}}\boldsymbol{v}^{\mathrm{dc}^\top}\vec{\boldsymbol{Y}}^\top\} \leq \vec{\bar{\boldsymbol{f}}}_{\max}, \tag{11a}$$

$$\overleftarrow{\boldsymbol{f}} = [\overleftarrow{\bar{\boldsymbol{x}}}]\,\mathrm{diag}\{\overleftarrow{\boldsymbol{L}}\boldsymbol{v}^{\mathrm{dc}}\boldsymbol{v}^{\mathrm{dc}^\top}\overleftarrow{\boldsymbol{Y}}^\top\} \leq \overleftarrow{\bar{\boldsymbol{f}}}_{\max}, \tag{11b}$$

and constrained by thermal limits of the line. Additionally, nodal voltages and power injections of the DC grid should be bounded as follows:

$$\boldsymbol{v}^{\mathrm{dc}}_{\min} \leq |\boldsymbol{v}^{\mathrm{dc}}| \leq \boldsymbol{v}^{\mathrm{dc}}_{\max}, \tag{12}$$

$$\boldsymbol{p}^{\mathrm{dc}}_{\min} \leq \boldsymbol{p}^{\mathrm{dc}} \leq \boldsymbol{p}^{\mathrm{dc}}_{\max}. \tag{13}$$

Constraints (12)–(13) enforce steady-state safety requirements. However, due to the mismatch of long-time dispatch interval and short-time power fluctuations, voltage limits in (12) need to be further restricted based on variations in load and generation, as well as the computational time delays in between droop set-point updates. In the following subsection, we formulate complementary voltage constraints that can further improve operational safety. With no loss of generality, for a simple DC node, without any VSC present, one can set $p^{\mathrm{dc}}_{\min} = p^{\mathrm{dc}}_{\max} = 0$.

E. MTDC Control Strategy

The generalized VSC voltage-droop characteristic [6] can be written as

$$\alpha_k v^{\mathrm{dc}}_k + \beta_k p^{\mathrm{dc}}_k + \gamma_k = 0, \qquad \forall k \in \mathcal{N}, \tag{14}$$

where p^{dc}_k and v^{dc}_k are the DC power and voltage set-points of the VSC at bus k. α_k, β_k, and γ_k denote the corresponding converter's voltage-droop parameters. In this paper, we assume that $\alpha_k = 1$. The voltage-droop slope is

$$\kappa_k \triangleq \beta_k = \frac{v^{\mathrm{dc}}_{\max_k} - v^{\mathrm{dc}}_{\min_k}}{p^{\mathrm{dc}}_{\max_k} - p^{\mathrm{dc}}_{\min_k}}, \tag{15}$$

and additionally, $\gamma_k = -v^{\mathrm{dc}}_k - \kappa_k p^{\mathrm{dc}}_k$. Equation (14) guarantees the optimal operation as long as updating droop set-points is fast enough compared to power fluctuations. However, due to the limits in computational speed, this assumption remains valid only if changes in load/generation are negligible. The

This article has been accepted for publication in a future issue of this journal, but has not been fully edited. Content may change prior to final publication. Citation information: DOI 10.1109/TPWRS.2021.3067025, IEEE Transactions on Power Systems

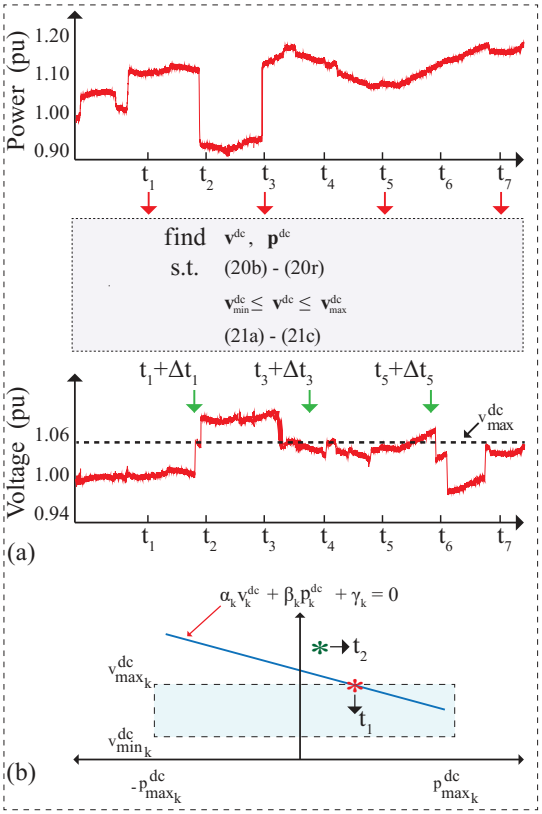

Fig. 2. Droop parameters optimized for the load/generation profile at time t_1 violates the safe operating region until the subsequent update that happens at time $t_3 + \Delta t_3$. (a) Load/generation profile and DC side voltage variation. (b) Generalized voltage-droop characteristics.

unwanted voltage deviation, caused by rapid changes, can be formulated as

$$\Delta v_k = \kappa_k \Delta p_k, \tag{16}$$

where $\Delta v_k = |v_k^{\rm dc}(t_1) - v_k^{\rm dc}(t_2)|$ and $\Delta p_k = |p_k^{\rm dc}(t_1) - p_k^{\rm dc}(t_2)|$. We seek to obtain conservative bounds on changes in DC voltage magnitudes, with the aim of ensuring smooth transition to the next operating point.

An illustrative example is provided in Figure 2 to highlight the necessity of this constraint. In Figure 2 (a), the optimizer collects the load profile at time t_1. Optimizing droop set-points requires a computational time, Δt_1. During this time, a noticeable variation in load/generation, as it happens at time t_2, invalidates obtained droop set-points until the subsequent update (at time $t_3 + \Delta t_3$). Thus, droop set-points found at time $t_1 + \Delta t_1$ become harmful for grid operation, particularly within the interval $[t_2, t_3 + \Delta t_3]$.

From a control perspective, one can design dead-ends on the droop controller [45] to prevent voltage violations caused by rapid changes. However, this could lead to a suboptimal solution since the corresponding converter starts in constant voltage/power control mode, without allowing the optimization framework to update other variables. Therefore, preventive droop control constraints should be integrated into optimization framework. Droop control set-points are obtained knowing whether safety limits are reached, while other variables are optimized accordingly. Herein, we offer the following additional voltage constraints, instead of (12), to guarantee a safe operation, i.e., DC voltage remains within the pre-described boundaries, under limited load/generation volatility:

$$v_{k_{\min}}^{\rm dc} + \Delta v_k = v_{k_{\min}}^{\rm dc} + \kappa_k \Delta p_k \le v_k^{\rm dc}, \tag{17}$$

$$v_{k_{\max}}^{\rm dc} - \Delta v_k = v_{k_{\max}}^{\rm dc} - \kappa_k \Delta p_k \ge v_k^{\rm dc}, \tag{18}$$

where Δp_k denotes the power variation in the DC side. A safe operating region can be devised such that corresponding voltage constraints allow power variation up to a specified level. This level can be decided based on the predefined percentage of an existing power injection, i.e., $\Delta p_k \le \mu_k p_k^{\rm dc}$.

IV. Topology-Cognizant OPF

A. Formulation of the Optimal Grid Topology

In Section III, we have modeled the operational and physical characteristics of a VSC-based MTDC grid. Herein, we devise an objective function that minimizes the total active power loss. The topology-cognizant OPF, with the aim of minimizing total loss, can be given as

$$\text{minimize} \quad \mathbf{1}_{|\mathcal{N}|}^\top \left(\boldsymbol{G}^\top \boldsymbol{p}^{\rm g} - \boldsymbol{D}^\top \boldsymbol{p}^{\rm d} \right) \tag{19a}$$

$$\text{subject to} \quad \text{real}\{\boldsymbol{s}^{\rm ac}\} + \boldsymbol{p}^{\rm dc} + \boldsymbol{a} + [\boldsymbol{b}]|\boldsymbol{i}^{\rm ac}| + [\boldsymbol{c}]|\boldsymbol{i}^{\rm ac}|^2 = \mathbf{0} \tag{19b}$$

$$|\boldsymbol{v}_{\rm c}^{\rm ac}| \le \sqrt{\frac{3}{2}} m \boldsymbol{v}^{\rm dc} \tag{19c}$$

$$\boldsymbol{s}^{\rm ac} = [\boldsymbol{v}_{\rm c}^{\rm ac}] \left([\boldsymbol{z}]^{-1} (\boldsymbol{v}_{\rm c}^{\rm ac} - \boldsymbol{v}_{\rm f}^{\rm ac}) \right)^* \tag{19d}$$

$$\boldsymbol{p}_{\min}^{\rm ac} \le \text{real}\{\boldsymbol{s}^{\rm ac}\} \le \boldsymbol{p}_{\max}^{\rm ac} \tag{19e}$$

$$\boldsymbol{q}_{\min}^{\rm ac} \le \text{imag}\{\boldsymbol{s}^{\rm ac}\} \le \boldsymbol{q}_{\max}^{\rm ac} - [\bar{\boldsymbol{q}}^{\rm ac}]|\boldsymbol{v}_{\rm f}^{\rm ac}| \tag{19f}$$

$$\boldsymbol{i}^{\rm ac} = [\boldsymbol{z}]^{-1} (\boldsymbol{v}_{\rm c}^{\rm ac} - \boldsymbol{v}_{\rm f}^{\rm ac}) \tag{19g}$$

$$|\boldsymbol{i}^{\rm ac}| \le \boldsymbol{i}_{\max}^{\rm ac} \tag{19h}$$

$$\boldsymbol{G}^\top \boldsymbol{p}^{\rm g} - \boldsymbol{D}^\top \boldsymbol{p}^{\rm d} = \text{real}\left\{ [\boldsymbol{v}_{\rm f}^{\rm ac}] \left([\boldsymbol{z}]^{-1} (\boldsymbol{v}_{\rm f}^{\rm ac} - \boldsymbol{v}_{\rm c}^{\rm ac}) \right)^* \right\} \tag{19i}$$

$$\boldsymbol{p}_{\min}^{\rm g} \le \boldsymbol{p}^{\rm g} \le \boldsymbol{p}_{\max}^{\rm g} \tag{19j}$$

$$\boldsymbol{v}_{\rm f_{\min}}^{\rm ac} \le |\boldsymbol{v}_{\rm f}^{\rm ac}| \le \boldsymbol{v}_{\rm f_{\max}}^{\rm ac} \tag{19k}$$

$$\boldsymbol{p}^{\rm dc} = \vec{\boldsymbol{L}}^\top \vec{\boldsymbol{f}} + \overleftarrow{\boldsymbol{L}}^\top \overleftarrow{\boldsymbol{f}} \tag{19l}$$

$$\boldsymbol{p}_{\min}^{\rm dc} \le \boldsymbol{p}^{\rm dc} \le \boldsymbol{p}_{\max}^{\rm dc} \tag{19m}$$

$$|\vec{\boldsymbol{f}} - \text{diag}\{\vec{\boldsymbol{L}}\, \boldsymbol{v}^{\rm dc} \boldsymbol{v}^{\rm dc^\top} \vec{\boldsymbol{Y}}^\top\}| \le M(1 - \vec{\boldsymbol{x}}) \tag{19n}$$

$$|\overleftarrow{\boldsymbol{f}} - \text{diag}\{\overleftarrow{\boldsymbol{L}}\, \boldsymbol{v}^{\rm dc} \boldsymbol{v}^{\rm dc^\top} \overleftarrow{\boldsymbol{Y}}^\top\}| \le M(1 - \vec{\boldsymbol{x}}) \tag{19o}$$

$$|\vec{\boldsymbol{f}}| \le [\vec{\boldsymbol{f}}_{\max}]\, \vec{\boldsymbol{x}} \tag{19p}$$

$$|\overleftarrow{\boldsymbol{f}}| \le [\vec{\boldsymbol{f}}_{\max}]\, \vec{\boldsymbol{x}} \tag{19q}$$

$$\vec{\boldsymbol{x}}_{\min} \le \vec{\boldsymbol{x}} \le \vec{\boldsymbol{x}}_{\max} \tag{19r}$$

$$\boldsymbol{v}_{\min}^{\rm dc} + [\boldsymbol{\kappa}][\boldsymbol{\mu}]\boldsymbol{p}^{\rm dc} \le \boldsymbol{v}^{\rm dc} \le \boldsymbol{v}_{\max}^{\rm dc} - [\boldsymbol{\kappa}][\boldsymbol{\mu}]\boldsymbol{p}^{\rm dc} \tag{19s}$$

$$\text{variables} \quad \boldsymbol{v}^{\rm dc}, \boldsymbol{p}^{\rm dc} \in \mathbb{R}^{|\mathcal{N}|}; \quad \boldsymbol{v}_{\rm c}^{\rm ac}, \boldsymbol{v}_{\rm f}^{\rm ac}, \boldsymbol{i}^{\rm ac}, \boldsymbol{s}^{\rm ac} \in \mathbb{C}^{|\mathcal{N}|}$$
$$\boldsymbol{p}^{\rm g} \in \mathbb{R}^{|\mathcal{G}|} \quad ; \quad \vec{\boldsymbol{f}}, \overleftarrow{\boldsymbol{f}} \in \mathbb{R}^{|\mathcal{L}|}; \quad \vec{\boldsymbol{x}} \in \{0,1\}^{|\mathcal{L}|}$$

where vectors $\boldsymbol{q}_{\min}^{\rm ac}$, $\boldsymbol{q}_{\max}^{\rm ac}$, and $\bar{\boldsymbol{q}}^{\rm ac}$ are set such that (19f) concludes (5). The topology-cognizant OPF formulation (19) suffers from (i) non-convex power balance and flow equations

(19d), (19i), (19n) and (19o), (ii) non-convex converter loss equations (19b), and (iii) the existence of binary variables, (19r), standing for the lines' statuses. The non-convex power flow equations corresponding to binary variables in (11a) and (11b) are relaxed using disjunctive inequalities, big-M reformulation, to (19n) and (19o), respectively. The big-M reformulation requires the determination of a sufficiently large multiplier (the big-M value) to ensure the equivalency to the original formulation when a transmission line is opened, $\vec{x}_l = 0$, [46], [47]. Nonlinear components, namely, $\boldsymbol{v}^{\rm dc}\boldsymbol{v}^{\rm dc^\top}$, $|\boldsymbol{v}_{\rm f}^{\rm ac}|$, $|\boldsymbol{v}_{\rm f}^{\rm ac}|^2$, $|\boldsymbol{v}_{\rm c}^{\rm ac}|^2$, $\mathrm{diag}\{\boldsymbol{v}_{\rm c}^{\rm ac}\boldsymbol{v}_{\rm f}^{\rm ac^*}\}$ and $|\boldsymbol{i}^{\rm ac}|$ can be convexified via conic and parabolic inequalities.

B. Formulation of the Lifted Problem

The topology-cognizant OPF problem in (19) is non-convex due to the non-linear constraints (19b), (19d), (19i), (19n) and (19o). These nonlinear components are $|\boldsymbol{i}^{\rm ac}|$ and $|\boldsymbol{i}^{\rm ac}|^2$ in (19b), $|\boldsymbol{v}_{\rm c}^{\rm ac}|^2$ and $\mathrm{diag}\{\boldsymbol{v}_{\rm c}^{\rm ac}\boldsymbol{v}_{\rm f}^{\rm ac^*}\}$ in (19d), $|\boldsymbol{v}_{\rm f}^{\rm ac}|^2$ and $\mathrm{diag}\{\boldsymbol{v}_{\rm c}^{\rm ac}\boldsymbol{v}_{\rm f}^{\rm ac^*}\}$ in (19i), and $\boldsymbol{v}^{\rm dc}\boldsymbol{v}^{\rm dc^\top}$ in (19n)-(19o). Each of these nonlinear components can be cast linearly by lifting the problem into a higher dimensional space. To this end, the nonlinear components are replaced with new auxiliary variables: $\boldsymbol{\phi}^{\rm ac} = |\boldsymbol{i}^{\rm ac}|$ and $\boldsymbol{t}^{\rm ac} = |\boldsymbol{i}^{\rm ac}|^2$ in (19b), $\boldsymbol{w}_{\rm cc}^{\rm ac} = |\boldsymbol{v}_{\rm c}^{\rm ac}|^2$ and $\boldsymbol{w}_{\rm cf}^{\rm ac} = \mathrm{diag}\{\boldsymbol{v}_{\rm c}^{\rm ac}\boldsymbol{v}_{\rm f}^{\rm ac^*}\}$ in (19d), $\boldsymbol{w}_{\rm ff}^{\rm ac} = |\boldsymbol{v}_{\rm f}^{\rm ac}|^2$ and $\boldsymbol{w}_{\rm cf}^{\rm ac} = \mathrm{diag}\{\boldsymbol{v}_{\rm c}^{\rm ac}\boldsymbol{v}_{\rm f}^{\rm ac^*}\}$ in (19i), and $\boldsymbol{W}^{\rm dc} = \boldsymbol{v}^{\rm dc}\boldsymbol{v}^{\rm dc^\top}$ in (19n) and (19o).

With the help of these auxiliary variables, $\boldsymbol{W}^{\rm dc} \in \mathbb{S}^{|\mathcal{N}|}$, $\boldsymbol{\phi}^{\rm ac}, \boldsymbol{t}^{\rm ac}, \boldsymbol{w}_{\rm cc}^{\rm ac}, \boldsymbol{w}_{\rm ff}^{\rm ac} \in \mathbb{R}^{|\mathcal{N}|}$, and $\boldsymbol{w}_{\rm cf}^{\rm ac} \in \mathbb{C}^{|\mathcal{N}|}$, the lifted problem can be formulated as

$$\text{minimize} \quad \mathbf{1}_{|\mathcal{N}|}^\top \left(\boldsymbol{G}^\top \boldsymbol{p}^{\rm g} - \boldsymbol{D}^\top \boldsymbol{p}^{\rm d}\right) \tag{20a}$$

$$\text{subject to} \quad \mathrm{real}\{\boldsymbol{s}^{\rm ac}\} + \boldsymbol{p}^{\rm dc} + \boldsymbol{a} + [\boldsymbol{b}]\boldsymbol{\phi}^{\rm ac} + [\boldsymbol{c}]\boldsymbol{t}^{\rm ac} = \mathbf{0} \tag{20b}$$

$$0 \le \boldsymbol{w}_{\rm cc}^{\rm ac} \le \frac{3}{2}\mathrm{diag}\{\boldsymbol{W}^{\rm dc}\} \tag{20c}$$

$$\boldsymbol{s}^{\rm ac} = \left([\boldsymbol{z}]^{-1}\right)^* (\boldsymbol{w}_{\rm cc}^{\rm ac} - \boldsymbol{w}_{\rm cf}^{\rm ac}) \tag{20d}$$

$$\boldsymbol{p}_{\min}^{\rm ac} \le \mathrm{real}\{\boldsymbol{s}^{\rm ac}\} \le \boldsymbol{p}_{\max}^{\rm ac} \tag{20e}$$

$$\boldsymbol{q}_{\min}^{\rm ac} \le \mathrm{imag}\{\boldsymbol{s}^{\rm ac}\} \le \boldsymbol{q}_{\max}^{\rm ac} - [\bar{\boldsymbol{q}}^{\rm ac}]|\boldsymbol{v}_{\rm f}^{\rm ac}| \tag{20f}$$

$$\boldsymbol{t}^{\rm ac} = [|\boldsymbol{z}|]^{-2}(\boldsymbol{w}_{\rm cc}^{\rm ac} + \boldsymbol{w}_{\rm ff}^{\rm ac} - 2\mathrm{real}\{\boldsymbol{w}_{\rm cf}^{\rm ac}\}) \tag{20g}$$

$$\boldsymbol{t}^{\rm ac} \le (\boldsymbol{i}_{\max}^{\rm ac})^2 \tag{20h}$$

$$\boldsymbol{G}^\top \boldsymbol{p}^{\rm g} - \boldsymbol{D}^\top \boldsymbol{p}^{\rm d} = \mathrm{real}\{[\boldsymbol{z}]^{-1}(\boldsymbol{w}_{\rm ff}^{\rm ac} - \boldsymbol{w}_{\rm cf}^{\rm ac})^*\} \tag{20i}$$

$$\boldsymbol{p}_{\min}^{\rm g} \le \boldsymbol{p}^{\rm g} \le \boldsymbol{p}_{\max}^{\rm g} \tag{20j}$$

$$(\boldsymbol{v}_{\rm f_{\min}}^{\rm ac})^2 \le \boldsymbol{w}_{\rm ff}^{\rm ac} \le (\boldsymbol{v}_{\rm f_{\max}}^{\rm ac})^2 \tag{20k}$$

$$\boldsymbol{p}^{\rm dc} = \vec{\boldsymbol{L}}^\top \vec{\boldsymbol{f}} + \overleftarrow{\boldsymbol{L}}^\top \overleftarrow{\boldsymbol{f}} \tag{20l}$$

$$\boldsymbol{p}_{\min}^{\rm dc} \le \boldsymbol{p}^{\rm dc} \le \boldsymbol{p}_{\max}^{\rm dc} \tag{20m}$$

$$|\vec{\boldsymbol{f}} - \mathrm{diag}\{\vec{\boldsymbol{L}}\, \boldsymbol{W}^{\rm dc} \vec{\boldsymbol{Y}}^\top\}| \le M(1 - \vec{\boldsymbol{x}}) \tag{20n}$$

$$|\overleftarrow{\boldsymbol{f}} - \mathrm{diag}\{\overleftarrow{\boldsymbol{L}}\, \boldsymbol{W}^{\rm dc} \overleftarrow{\boldsymbol{Y}}^\top\}| \le M(1 - \overleftarrow{\boldsymbol{x}}) \tag{20o}$$

$$|\vec{\boldsymbol{f}}| \le [\vec{\boldsymbol{f}}_{\max}]\, \vec{\boldsymbol{x}} \tag{20p}$$

$$|\overleftarrow{\boldsymbol{f}}| \le [\overleftarrow{\boldsymbol{f}}_{\max}]\, \overleftarrow{\boldsymbol{x}} \tag{20q}$$

$$\vec{\boldsymbol{x}}_{\min} \le \vec{\boldsymbol{x}} \le \vec{\boldsymbol{x}}_{\max} \tag{20r}$$

$$\boldsymbol{v}_{\min}^{\rm dc} + [\boldsymbol{\kappa}][\boldsymbol{\mu}]\boldsymbol{p}^{\rm dc} \le \boldsymbol{v}^{\rm dc} \le \boldsymbol{v}_{\max}^{\rm dc} - [\boldsymbol{\kappa}][\boldsymbol{\mu}]\boldsymbol{p}^{\rm dc} \tag{20s}$$

$$\sqrt{\boldsymbol{t}^{\rm ac}} = \boldsymbol{\phi}^{\rm ac} = |\boldsymbol{i}^{\rm ac}| \tag{20t}$$

$$\begin{aligned}
&\sqrt{[\vec{\boldsymbol{L}}\mathrm{diag}\{\boldsymbol{W}^{\rm dc}\}]\, \overleftarrow{\boldsymbol{L}}\mathrm{diag}\{\boldsymbol{W}^{\rm dc}\}} = \mathrm{diag}\{\vec{\boldsymbol{L}}\boldsymbol{W}^{\rm dc}\overleftarrow{\boldsymbol{L}}^\top\}\\
&\mathrm{diag}\{(\vec{\boldsymbol{L}} - \overleftarrow{\boldsymbol{L}})\boldsymbol{W}^{\rm dc}(\vec{\boldsymbol{L}} - \overleftarrow{\boldsymbol{L}})^\top\} = \left(\vec{\boldsymbol{L}}\boldsymbol{v}^{\rm dc} - \vec{\boldsymbol{L}}\boldsymbol{v}^{\rm dc}\right)^2\\
&\mathrm{diag}\{(\vec{\boldsymbol{L}} + \overleftarrow{\boldsymbol{L}})\boldsymbol{W}^{\rm dc}(\vec{\boldsymbol{L}} + \overleftarrow{\boldsymbol{L}})^\top\} = \left(\vec{\boldsymbol{L}}\boldsymbol{v}^{\rm dc} + \vec{\boldsymbol{L}}\boldsymbol{v}^{\rm dc}\right)^2\\
&\mathrm{diag}\{\boldsymbol{W}^{\rm dc}\} = \left(\boldsymbol{v}^{\rm dc}\right)^2
\end{aligned} \tag{20u}$$

$$\begin{aligned}
&\sqrt{[\boldsymbol{w}_{\rm ff}^{\rm ac}]\boldsymbol{w}_{\rm cc}^{\rm ac}} = |\boldsymbol{w}_{\rm cf}^{\rm ac}|,\\
&\boldsymbol{w}_{\rm ff}^{\rm ac} + \boldsymbol{w}_{\rm cc}^{\rm ac} - 2\,\mathrm{real}\{\boldsymbol{w}_{\rm cf}^{\rm ac}\} = |\boldsymbol{v}_{\rm c}^{\rm ac} - \boldsymbol{v}_{\rm f}^{\rm ac}|^2,\\
&\boldsymbol{w}_{\rm ff}^{\rm ac} + \boldsymbol{w}_{\rm cc}^{\rm ac} + 2\,\mathrm{real}\{\boldsymbol{w}_{\rm cf}^{\rm ac}\} = |\boldsymbol{v}_{\rm c}^{\rm ac} + \boldsymbol{v}_{\rm f}^{\rm ac}|^2,\\
&\boldsymbol{w}_{\rm ff}^{\rm ac} + \boldsymbol{w}_{\rm cc}^{\rm ac} - 2\,\mathrm{imag}\{\boldsymbol{w}_{\rm cf}^{\rm ac}\} = |\boldsymbol{v}_{\rm c}^{\rm ac} + i\boldsymbol{v}_{\rm f}^{\rm ac}|^2,\\
&\boldsymbol{w}_{\rm ff}^{\rm ac} + \boldsymbol{w}_{\rm cc}^{\rm ac} + 2\,\mathrm{imag}\{\boldsymbol{w}_{\rm cf}^{\rm ac}\} = |\boldsymbol{v}_{\rm c}^{\rm ac} - i\boldsymbol{v}_{\rm f}^{\rm ac}|^2,\\
&\boldsymbol{w}_{\rm ff}^{\rm ac} = |\boldsymbol{v}_{\rm f}^{\rm ac}|^2, \qquad \boldsymbol{w}_{\rm cc}^{\rm ac} = |\boldsymbol{v}_{\rm c}^{\rm ac}|^2,
\end{aligned} \tag{20v}$$

$$\begin{aligned}
\text{variables} \quad & \boldsymbol{v}_{\rm c}^{\rm ac}, \boldsymbol{v}_{\rm f}^{\rm ac}, \boldsymbol{w}_{\rm cc}^{\rm ac}, \boldsymbol{w}_{\rm ff}^{\rm ac}, \boldsymbol{w}_{\rm cf}^{\rm ac}, \boldsymbol{s}^{\rm ac}, \boldsymbol{i}^{\rm ac} \in \mathbb{C}^{|\mathcal{N}|};\\
& \boldsymbol{W}^{\rm dc} \in \mathbb{S}^{|\mathcal{N}|};\ \boldsymbol{\phi}^{\rm ac}, \boldsymbol{t}^{\rm ac}, \boldsymbol{p}^{\rm dc} \in \mathbb{R}^{|\mathcal{N}|};\ \boldsymbol{p}^{\rm g} \in \mathbb{R}^{|\mathcal{G}|};\\
& \vec{\boldsymbol{f}}, \overleftarrow{\boldsymbol{f}} \in \mathbb{R}^{|\mathcal{L}|};\ \vec{\boldsymbol{x}} \in \{0,1\}^{|\mathcal{L}|}
\end{aligned}$$

The non-convexity of (19) is circumvented by lifting its nonlinear terms into the form of (20) while preserving the equivalency between the two formulations, with the help of additional constraints (20t)-(20v). Constraints (20t)-(20v) basically impose $\boldsymbol{\phi}^{\rm ac} = |\boldsymbol{i}^{\rm ac}|$, $\boldsymbol{t}^{\rm ac} = |\boldsymbol{i}^{\rm ac}|^2$, $\boldsymbol{W}^{\rm dc} = \boldsymbol{v}^{\rm dc}\boldsymbol{v}^{\rm dc^\top}$, $\boldsymbol{w}_{\rm cc}^{\rm ac} = |\boldsymbol{v}_{\rm c}^{\rm ac}|^2$, $\boldsymbol{w}_{\rm ff}^{\rm ac} = |\boldsymbol{v}_{\rm f}^{\rm ac}|^2$, and $\boldsymbol{w}_{\rm cf}^{\rm ac} = \mathrm{diag}\{\boldsymbol{v}_{\rm c}^{\rm ac}\boldsymbol{v}_{\rm f}^{\rm ac^*}\}$. On the other hand, the lifted matrix and vector equality constraints in (20t)-(20v) pose new sources of non-convexity, but they can be convexified via a transformation of equalities to inequalities.

C. Convex Relaxation

Motivated by [48], a MISOCP formulation can be readily obtained, by relaxing (20t)-(20v) into the following conic and parabolic inequalities:

$$\sqrt{\boldsymbol{t}^{\rm ac}} \ge \boldsymbol{\phi}^{\rm ac} \ge |\boldsymbol{i}^{\rm ac}| \tag{21a}$$

$$\begin{aligned}
&\sqrt{[\vec{\boldsymbol{L}}\mathrm{diag}\{\boldsymbol{W}^{\rm dc}\}]\, \overleftarrow{\boldsymbol{L}}\mathrm{diag}\{\boldsymbol{W}^{\rm dc}\}} \ge \mathrm{diag}\{\vec{\boldsymbol{L}}\boldsymbol{W}^{\rm dc}\overleftarrow{\boldsymbol{L}}^\top\}\\
&\mathrm{diag}\{(\vec{\boldsymbol{L}} - \overleftarrow{\boldsymbol{L}})\boldsymbol{W}^{\rm dc}(\vec{\boldsymbol{L}} - \overleftarrow{\boldsymbol{L}})^\top\} \ge (\vec{\boldsymbol{L}}\boldsymbol{v}^{\rm dc} - \vec{\boldsymbol{L}}\boldsymbol{v}^{\rm dc})^2\\
&\mathrm{diag}\{(\vec{\boldsymbol{L}} + \overleftarrow{\boldsymbol{L}})\boldsymbol{W}^{\rm dc}(\vec{\boldsymbol{L}} + \overleftarrow{\boldsymbol{L}})^\top\} \ge (\vec{\boldsymbol{L}}\boldsymbol{v}^{\rm dc} + \vec{\boldsymbol{L}}\boldsymbol{v}^{\rm dc})^2\\
&\mathrm{diag}\{\boldsymbol{W}^{\rm dc}\} \ge (\boldsymbol{v}^{\rm dc})^2
\end{aligned} \tag{21b}$$

$$\begin{aligned}
&\sqrt{[\boldsymbol{w}_{\rm ff}^{\rm ac}]\boldsymbol{w}_{\rm cc}^{\rm ac}} \ge |\boldsymbol{w}_{\rm cf}^{\rm ac}|,\\
&\boldsymbol{w}_{\rm ff}^{\rm ac} + \boldsymbol{w}_{\rm cc}^{\rm ac} - 2\,\mathrm{real}\{\boldsymbol{w}_{\rm cf}^{\rm ac}\} \ge |\boldsymbol{v}_{\rm c}^{\rm ac} - \boldsymbol{v}_{\rm f}^{\rm ac}|^2,\\
&\boldsymbol{w}_{\rm ff}^{\rm ac} + \boldsymbol{w}_{\rm cc}^{\rm ac} + 2\,\mathrm{real}\{\boldsymbol{w}_{\rm cf}^{\rm ac}\} \ge |\boldsymbol{v}_{\rm c}^{\rm ac} + \boldsymbol{v}_{\rm f}^{\rm ac}|^2,\\
&\boldsymbol{w}_{\rm ff}^{\rm ac} + \boldsymbol{w}_{\rm cc}^{\rm ac} - 2\,\mathrm{imag}\{\boldsymbol{w}_{\rm cf}^{\rm ac}\} \ge |\boldsymbol{v}_{\rm c}^{\rm ac} + i\boldsymbol{v}_{\rm f}^{\rm ac}|^2,\\
&\boldsymbol{w}_{\rm ff}^{\rm ac} + \boldsymbol{w}_{\rm cc}^{\rm ac} + 2\,\mathrm{imag}\{\boldsymbol{w}_{\rm cf}^{\rm ac}\} \ge |\boldsymbol{v}_{\rm c}^{\rm ac} - i\boldsymbol{v}_{\rm f}^{\rm ac}|^2,\\
&\boldsymbol{w}_{\rm ff}^{\rm ac} \ge |\boldsymbol{v}_{\rm f}^{\rm ac}|^2, \qquad \boldsymbol{w}_{\rm cc}^{\rm ac} \ge |\boldsymbol{v}_{\rm c}^{\rm ac}|^2,
\end{aligned} \tag{21c}$$

The resulting MISOCP-relaxed topology-cognizant OPF problem (20) with relaxed constraints (21a)-(21c) is compatible with the state-of-the-art branch-and-bound solvers which enables the search for binary variables.

D. Penalization

The convex relaxation given in (21a)-(21c) may sometimes lead to an inexact solution with infeasible points for the original nonconvex formulation. In order to ensure that (20t)-(20v) are satisfied, we incorporate a penalty function of the form

$$\rho_{\check{\boldsymbol{v}}^{\rm dc},\check{\boldsymbol{v}}_{\rm c}^{\rm ac},\check{\boldsymbol{v}}_{\rm f}^{\rm ac},\check{\boldsymbol{i}}^{\rm ac}}(\boldsymbol{W}^{\rm dc},\boldsymbol{v}^{\rm dc},\boldsymbol{w}_{\rm cc}^{\rm ac},\boldsymbol{v}_{\rm c}^{\rm ac},\boldsymbol{w}_{\rm ff}^{\rm ac},\boldsymbol{v}_{\rm f}^{\rm ac},\boldsymbol{t}^{\rm ac},\boldsymbol{i}^{\rm ac}) =$$

$$\eta^{\rm dc}\big({\rm tr}\{\boldsymbol{W}^{\rm dc}\} - 2(\check{\boldsymbol{v}}^{\rm dc})^{\top}\boldsymbol{v}^{\rm dc} + \|\check{\boldsymbol{v}}^{\rm dc}\|_2^2\big) + \tag{22a}$$

$$\eta_{\rm c}^{\rm ac}\big(\mathbf{1}_{|\mathcal{N}|}^{\top}\boldsymbol{w}_{\rm cc}^{\rm ac} - (\check{\boldsymbol{v}}_{\rm c}^{\rm ac})^{*}\boldsymbol{v}_{\rm c}^{\rm ac} - (\boldsymbol{v}_{\rm c}^{\rm ac})^{*}\check{\boldsymbol{v}}_{\rm c}^{\rm ac} + \|\check{\boldsymbol{v}}_{\rm c}^{\rm ac}\|_2^2\big) + \tag{22b}$$

$$\eta_{\rm f}^{\rm ac}\big(\mathbf{1}_{|\mathcal{N}|}^{\top}\boldsymbol{w}_{\rm ff}^{\rm ac} - (\check{\boldsymbol{v}}_{\rm f}^{\rm ac})^{*}\boldsymbol{v}_{\rm f}^{\rm ac} - (\boldsymbol{v}_{\rm f}^{\rm ac})^{*}\check{\boldsymbol{v}}_{\rm f}^{\rm ac} + \|\check{\boldsymbol{v}}_{\rm f}^{\rm ac}\|_2^2\big) + \tag{22c}$$

$$\eta_{\rm i}^{\rm ac}\big(\mathbf{1}_{|\mathcal{N}|}^{\top}\boldsymbol{t}^{\rm ac} - (\check{\boldsymbol{i}}^{\rm ac})^{*}\boldsymbol{i}^{\rm ac} - (\boldsymbol{i}^{\rm ac})^{*}\check{\boldsymbol{i}}^{\rm ac} + \|\check{\boldsymbol{i}}^{\rm ac}\|_2^2\big) \tag{22d}$$

into the objective of convex relaxation, where $(\check{\boldsymbol{v}}^{\rm dc},\check{\boldsymbol{v}}_{\rm c}^{\rm ac},\check{\boldsymbol{v}}_{\rm f}^{\rm ac},\check{\boldsymbol{i}}^{\rm ac}) \in \mathbb{R}^{|\mathcal{N}|}\times\mathbb{R}^{|\mathcal{C}|}\times\mathbb{R}^{|\mathcal{C}|}\times\mathbb{R}^{|\mathcal{C}|}$ can be any arbitrary initial point. As shown in [48], [49], the proper selection of penalty coefficients $\eta^{\rm dc},\eta_{\rm c}^{\rm ac},\eta_{\rm f}^{\rm ac},\eta_{\rm i}^{\rm ac}\geq 0$ guarantees the recovery of near-optimal feasible points. In the following section, we show that the simple choice of parameters

$$\check{\boldsymbol{v}}^{\rm dc} = \check{\boldsymbol{v}}_{\rm c}^{\rm ac} = \check{\boldsymbol{v}}_{\rm f}^{\rm ac} = \check{\boldsymbol{i}}^{\rm ac} = 0, \tag{23a}$$

$$\eta^{\rm dc} = 10^{-4}, \qquad \eta_{\rm i}^{\rm ac} = 10^{-5}, \qquad \eta_{\rm c}^{\rm ac} = \eta_{\rm f}^{\rm ac} = 0, \tag{23b}$$

can reliably solve the original non-convex problem in practice. The proposed algorithm is not sensitive to the choice of penalty parameters, they only need to be larger than a threshold [49].

V. Case Studies

A. System Setup

The modified CIGRE B4 DC grid benchmark [50], equipped with switches to open/close transmission lines, is illustrated in Figure 3. This MTDC grid is emulated in a HIL platform, with two dSPACE DS1202 MicroLabBoxes to implement droop controllers for individual VSCs, and two Typhoon HIL604 units to emulate VSCs and transmission lines, as shown in Figure 4. The flowchart given in Figure 5 shows the implementation of topology-cognizant OPF in a HIL environment. The TCP/IP link between Typhoon HIL/MATLAB/dSPACE MicroLabBoxes shares the load, set-point information, and the status of switching devices at every five second. A PC with 16-core, Xeon processor, and 256 GB RAM solves the proposed algorithm using the CVX v2.1 [51], and the conic mixed-integer solver GUROBI v8.0.1 [52]. In the following studies, four time intervals, $[0\text{s},120\text{s}]$, $[120\text{s},220\text{s}]$, $[220\text{s},320\text{s}]$, and $[320\text{s},420\text{s}]$, are considered.

The rated power of each VSC is 1200 MW, which is also chosen as a base power in the calculation of per unit values. Meanwhile, the base voltage is set to 380 kV. Variable loads are attached to bus 1 and bus 4. The bounds on power constraints for AC and DC sides are $p_{\min_k}^{\rm dc} = p_{\min_k}^{\rm ac} = -1200$ MW

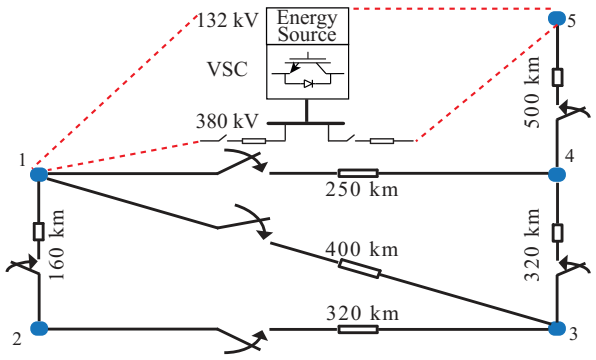

Fig. 3. The modified CIGRE B4 DC grid equipped with line switches. DC cable resistance for +/-400 kV is 0.0095 Ω/km.

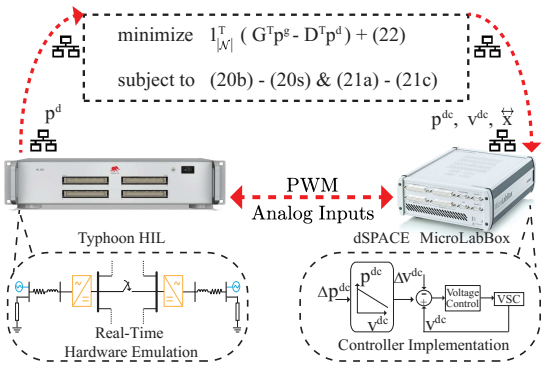

Fig. 4. Topology-cognizant OPF testbed on a real-time HIL platform has hardware emulation (Typhoon HIL), controller implementation (dSPACE), and TCP/IP communication link.

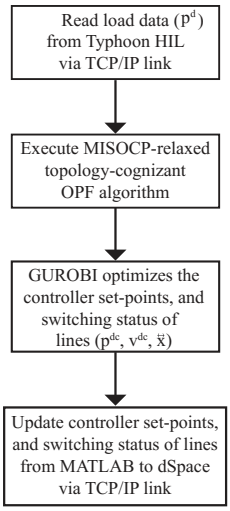

Fig. 5. Flowchart of the proposed topology-cognizant OPF algorithm.

This article has been accepted for publication in a future issue of this journal, but has not been fully edited. Content may change prior to final publication. Citation information: DOI 10.1109/TPWRS.2021.3067025, IEEE Transactions on Power Systems

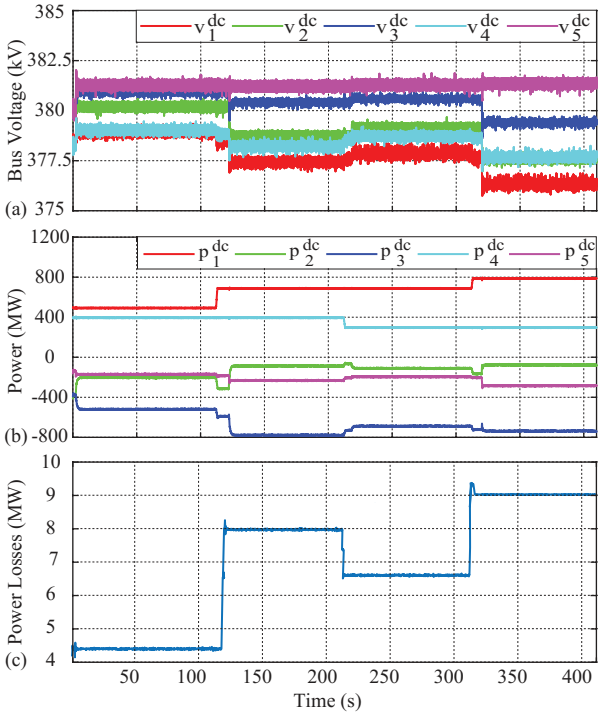

Fig. 6. MTDC operation with droop control under varying load: (a) DC side voltage variation, (b) DC side power variation, and (c) Total power losses.

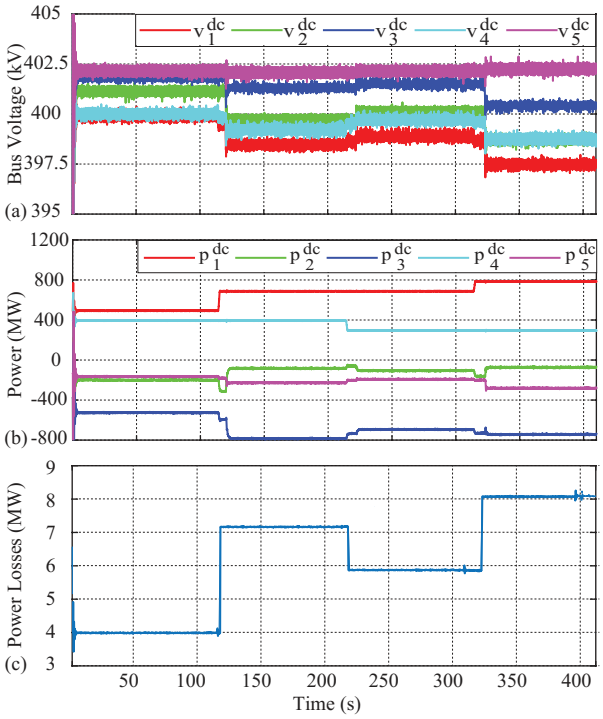

Fig. 7. MTDC operation with static OPF under varying load: (a) DC side voltage variation, (b) DC side power variation, and (c) Total power losses.

and $p^{\text{dc}}_{\max_k} = p^{\text{ac}}_{\max_k} = 1200\,\text{MW}$ for every VSC at bus $k \in \mathcal{N}$. The loss coefficients in (1) are $a_k = 2.65 \times 10^{-5}$, $b_k = 3.7 \times 10^{-5}$, and $c_k = 3.6 \times 10^{-5}$ for every VSC at bus $k \in \mathcal{N}$. The converter constant and nominal apparent power in (5) are $m_b = 0.6$ and $|\bar{s}^{\text{ac}}| = 1$ pu, respectively. Phase-reactor parameters in (5) are $r_k = 2.5 \times 10^{-6}$ and $x_k = 4 \times 10^{-4}$ for every $k \in \mathcal{N}$. VSC parameters are $i^{\text{ac}}_{\text{c}\max} = 1.0526$ pu and $v^{\text{ac}}_{\text{c}\max} = 1.05$ pu. The maximum modulation factor in (2) is $m = 1$. The voltage bounds are 0.94 pu (352.7 kV) and 1.06 pu (402.8 kV). The lines are rated at $\vec{f}_{l_{\max}} = 0.25$ pu (300 MW) for every $l \in \mathcal{L}$. The big-M value in (19) and (20) is $M = 500$. Safety constraint coefficients in (20s) are $\mu_k = 10\%$ and $\kappa_k = 5\%$ for every VSC at bus $k \in \mathcal{N}$. Penalty coefficients in (22) are chosen from (23). A solution is regarded feasible when the maximum mismatch between the right and left sides of inequalities in (21a)-(21c) is less than 10^{-6}.

B. MTDC Grid Operation with Static OPF

Static OPF refers to the problem (20) with a connected grid, $\vec{x}_{l_{\min}} = \vec{x}_{l_{\max}} = 1$ for every $l \in \mathcal{L}$. If OPF results do not update the set-points of the local droop controller, they arrive at a feasible operating condition shown in Figure 6. The primary aim of a local controller is to maintain stable operation of a VSC in meeting the load demand as well as voltage-power tracking. Optimal operation of the MTDC grid cannot be accomplished with the local controllers alone and requires upper-level optimizer to reduce the total loss. The total loss obtained via local controllers and static OPF are given in Table I. With the implementation of the static OPF result, shown in Figure 7, around 10% reduction in loss is reported compared to results obtained via local droop controllers alone. The average computation time to solve the static OPF and update droop set-points is 1.4 s.

TABLE I
TOTAL LOSSES WITH DIFFERENT APPROACHES (MW)

Method \ Time interval (s)	0-120	120-220	220-320	320-420
Local droop controller	4.40	8.00	6.50	9.00
Static OPF	3.97	7.16	5.86	8.08
Topology-cognizant OPF without the safety constraints (20) without (20s)	3.78	6.19	5.11	7.11
Topology-cognizant OPF with the safety constraints (20) with (20s)	3.80	6.22	5.14	7.13

C. MTDC Grid Operation with Topology-cognizant OPF

In this section, we see the effect of including the additional safety constraints, (20s), in the problem formulation, (20). Existing methodologies suffer from voltage violations caused by power fluctuation in between two droop set-point updates. Herein, additional safety constraints, (20s), are validated to remedy these voltage violations. The formulation (20), with and without the constraints in (20s), finds the optimal grid topology with the goal of reducing the total loss. The outcome of topology-cognizant OPF problem without voltage safety limits in (20s) further reduces the total loss by 4.79%, 13.54%, 12.80%, and 12.00% for the four time intervals as compared to the static OPF scenarios. Based on the outcome of (20)

This article has been accepted for publication in a future issue of this journal, but has not been fully edited. Content may change prior to final publication. Citation information: DOI 10.1109/TPWRS.2021.3067025, IEEE Transactions on Power Systems

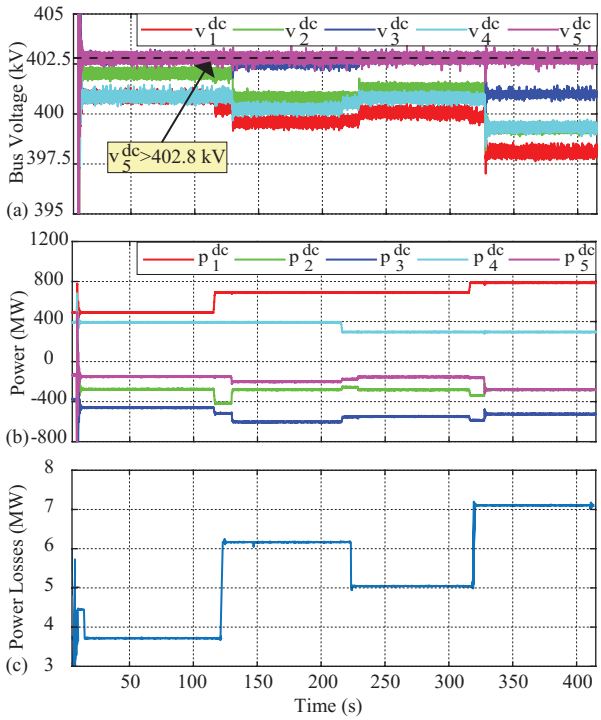

Fig. 8. MTDC operation with topology-cognizant OPF disregarding voltage safety constraints in (20s). The variations in load/generation have DC voltage at bus 5 violate the safety limit: (a) DC side voltage variation (dotted line shows the safety limit, $v_{\max}^{\text{dc}} = 402.8$ kV), (b) DC side power variation, and (c) Total power losses.

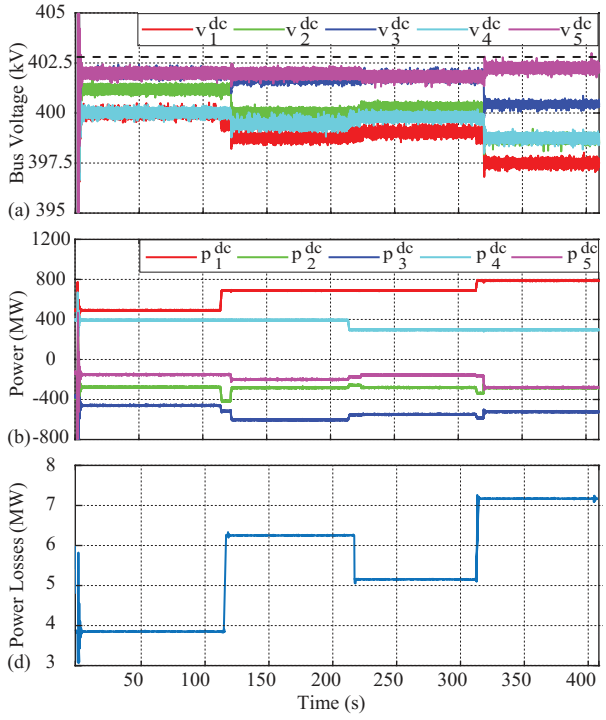

Fig. 9. MTDC operation with topology-cognizant OPF considering the voltage safety constraints in (20s): (a) DC side voltage variation (dotted line shows the safety limit, $v_{\max}^{\text{dc}} = 402.8$ kV), (b) DC side power variation, and (c) Total power losses.

(except (20s)), $\vec{x}_{2-3}$ is always disconnected, while $\vec{x}_{1-4}$ is disconnected only during $[0\text{s}, 120\text{s}]$ time interval. Even though the total loss is further reduced, the voltage safety limits are violated at bus 5 due to load fluctuations and the computation time involved in updating droop set-points, see Figure 8 (a). Additional safety constraints in (20s) mitigate any voltage violation in response to power fluctuations in between two droop set-points updates as shown in Figure 9 (a). This safer operation comes with a slightly higher total loss compared to the case ignoring (20s); Nevertheless, it still offers remarkable reduction in total loss as compared to the static OPF. The total loss obtained by the topology-cognizant OPF with and without the constraints in (20s) are given in Table I. Total losses for different loading profiles are about 0.42%, 0.57%, 0.52%, and 0.65% of the total load demand for the four time intervals, respectively. The converter losses obtained from convex relaxation approach are about 7.31%, 4.71%, 5.65%, and 4.18% of the total loss in corresponding intervals. Updating droop set-points, that are sent to VSCs every five second, takes around 2.5 s.

D. Deployment on Larger Networks

In this section, we have conducted a series of numerical experiments on a collection of modified IEEE 14, 30, and 57-bus benchmarks to study the scalability of the proposed algorithm in (20). In practice, MTDC networks tend to have only a few nodes [53]–[57]. First, we study the static OPF problem, where $\vec{x}_{l_{\min}} = \vec{x}_{l_{\max}} = 1$ for every $l \in \mathcal{L}$, for IEEE 14, 30, and 57-bus benchmarks, that have been modified to MTDC networks by adding VSCs to every bus and switches to every transmission line, and making these lines resistive. Total losses obtained are 0.00550 pu, 0.00860 pu, and 0.02030 pu, respectively. The computation times are roughly 1.59, 3.92, and 10.21 s, respectively. We then study the topology-cognizant problem where, for the modified IEEE 14, 30, and 57-bus benchmarks, 4 out of 20, 13 out of 41, and 14 out of 80 transmission lines are disconnected, respectively. The total losses, respectively, are reduced to 0.00538 pu, 0.00813 pu, and 0.0168 pu, which are 2.18%, 5.46%, 17.24% less compared to those acquired using the static OPF. The status of transmission lines, voltage and power levels at each bus for the modified IEEE 14, 30, and 57-bus benchmarks take 18, 42, and 136s, respectively, on average, to be determined. Figure 10 illustrates the topology of the IEEE 57-bus system before and after applying the topology-cognizant OPF algorithm.

VI. Conclusion

This paper offers a convex optimization framework to solve the grid topology-cognizant OPF problem for MTDC grids. It provides local voltage and power set-points for droop controllers of VSCs as well as the operational status of transmission lines. Additional constraints, that sustain safe operation in response to the power fluctuation in between two droop updates, are integrated into the proposed formulation. The resulting formulation has computational difficulties due to the non-convex power balance, flow and converter loss equations as well as the inclusion of binary decision variables. Convex

This article has been accepted for publication in a future issue of this journal, but has not been fully edited. Content may change prior to final publication. Citation information: DOI 10.1109/TPWRS.2021.3067025, IEEE Transactions on Power Systems

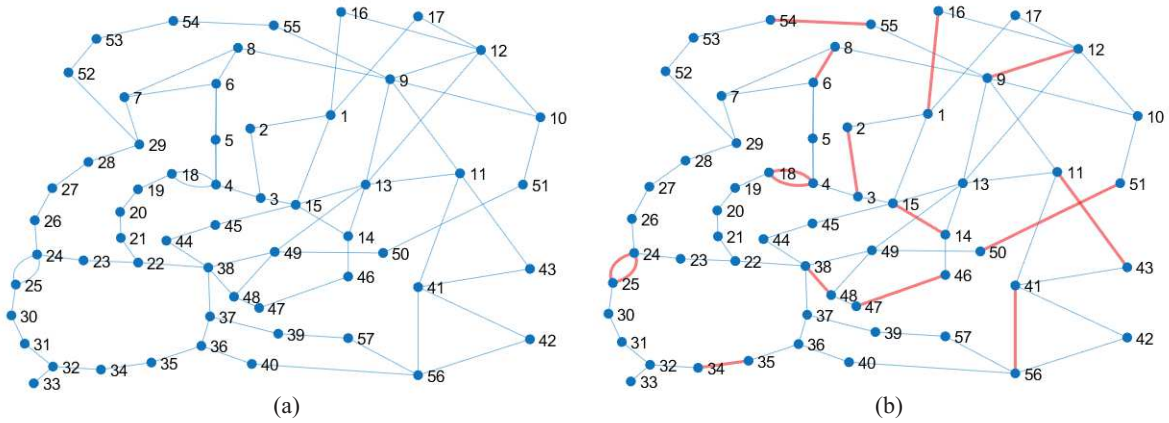

Fig. 10. a) IEEE 57-bus system topology, and b) the topology upon enforcing the topology-cognizant OPF, red-colored lines refer to disconnected transmission lines.

relaxation methods are utilized to transform this problem into a tractable model so that it can be executed with off-the-shelf solvers. Experimental and numerical results validate the practicability and efficacy of the proposed approach.

ACKNOWLEDGMENT

We are grateful to dSPACE Inc. and Typhoon HIL Inc. for letting us to use their products' images.

REFERENCES

[1] M. Andreasson, D. V. Dimarogonas, H. Sandberg, and K. H. Johansson, "Distributed controllers for multiterminal hvdc transmission systems," *IEEE Transactions on Control of Network Systems*, vol. 4, no. 3, pp. 564–574, Sep. 2017.

[2] D. Van Hertem and M. Ghandhari, "Multi-terminal vsc hvdc for the european supergrid: Obstacles," *Renewable and sustainable energy reviews*, vol. 14, no. 9, pp. 3156–3163, 2010.

[3] A. Yazdani and R. Iravani, *Voltage-sourced converters in power systems*. Wiley Online Library, 2010, vol. 34.

[4] N. Yousefpoor, S. Kim, and S. Bhattacharya, "Multi-terminal dc grid control under loss of terminal station," in *2014 IEEE Energy Conversion Congress and Exposition (ECCE)*, Sept 2014, pp. 744–749.

[5] J. Beerten, S. Cole, and R. Belmans, "Modeling of multi-terminal vsc hvdc systems with distributed dc voltage control," *IEEE Transactions on Power Systems*, vol. 29, no. 1, pp. 34–42, Jan 2014.

[6] K. Rouzbehi, A. Miranian, J. I. Candela, A. Luna, and P. Rodriguez, "A generalized voltage droop strategy for control of multiterminal dc grids," *IEEE Transactions on Industry Applications*, vol. 51, no. 1, pp. 607–618, Jan 2015.

[7] C. Gavriluta, J. I. Candela, J. Rocabert, A. Luna, and P. Rodriguez, "Adaptive droop for control of multiterminal dc bus integrating energy storage," *IEEE Transactions on Power Delivery*, vol. 30, no. 1, pp. 16–24, Feb 2015.

[8] S. Shin, P. Hart, T. Jahns, and V. M. Zavala, "A hierarchical optimization architecture for large-scale power networks," *IEEE Transactions on Control of Network Systems*, vol. 6, no. 3, pp. 1004–1014, Sep. 2019.

[9] Q. Nguyen, G. Todeschini, and S. Santoso, "Power flow in a multi-frequency hvac and hvdc system: Formulation, solution, and validation," *IEEE Transactions on Power Systems*, vol. 34, no. 4, pp. 2487–2497, July 2019.

[10] M. A. Abdelwahed and E. F. El-Saadany, "Power sharing control strategy of multiterminal VSC-HVDC transmission systems utilizing adaptive voltage droop," *IEEE Transactions on Sustainable Energy*, vol. 8, no. 2, pp. 605–615, April 2017.

[11] T. M. Haileselassie and K. Uhlen, "Impact of dc line voltage drops on power flow of mtdc using droop control," *IEEE Transactions on Power Systems*, vol. 27, no. 3, pp. 1441–1449, Aug 2012.

[12] L. Xiao, Z. Xu, T. An, and Z. Bian, "Improved analytical model for the study of steady state performance of droop-controlled VSC-MTDC systems," *IEEE Transactions on Power Systems*, 2016.

[13] A. Nikoobakht, J. Aghaei, T. Niknam, V. Vahidinasab, H. Farahmand, and M. Korpås, "Towards robust opf solution strategy for the future ac/dc grids: case of VSC-HVDC-connected offshore wind farms," *IET Renewable Power Generation*, vol. 12, no. 6, pp. 691–701, 2018.

[14] F. Sun, J. Ma, M. Yu, and W. Wei, "A robust optimal coordinated droop control method for multiple vscs in ac-dc distribution network," *IEEE Transactions on Power Systems*, pp. 1–1, 2019.

[15] B. Li, Q. Li, Y. Wang, W. Wen, B. Li, and L. Xu, "A novel method to determine droop coefficients of dc voltage control for VSC-MTDC system," *IEEE Transactions on Power Delivery*, pp. 1–1, 2020.

[16] C. Gavriluta, I. Candela, A. Luna, A. Gomez-Exposito, and P. Rodriguez, "Hierarchical control of hv-mtdc systems with droop-based primary and opf-based secondary," *IEEE Transactions on Smart Grid*, vol. 6, no. 3, pp. 1502–1510, May 2015.

[17] W. Feng, L. A. Tuan, L. B. Tjernberg, A. Mannikoff, and A. Bergman, "A new approach for benefit evaluation of multiterminal vsc–hvdc using a proposed mixed ac/dc optimal power flow," *IEEE Transactions on Power Delivery*, vol. 29, no. 1, pp. 432–443, Feb 2014.

[18] S. H. Low, "Convex relaxation of optimal power flow-part i: Formulations and equivalence," *IEEE Transactions on Control of Network Systems*, vol. 1, no. 1, pp. 15–27, March 2014.

[19] S. H. Low, "Convex relaxation of optimal power flow—part ii: Exactness," *IEEE Transactions on Control of Network Systems*, vol. 1, no. 2, pp. 177–189, June 2014.

[20] S. Bahrami, F. Therrien, V. W. S. Wong, and J. Jatskevich, "Semidefinite relaxation of optimal power flow for ac–dc grids," *IEEE Transactions on Power Systems*, vol. 32, no. 1, pp. 289–304, Jan 2017.

[21] M. Baradar, M. R. Hesamzadeh, and M. Ghandhari, "Second-order cone programming for optimal power flow in VSC-Type ac-dc grids," *IEEE Transactions on Power Systems*, vol. 28, no. 4, pp. 4282–4291, Nov 2013.

[22] H. Ergun, J. Dave, D. Van Hertem, and F. Geth, "Optimal power flow for ac–dc grids: Formulation, convex relaxation, linear approximation, and implementation," *IEEE Transactions on Power Systems*, vol. 34, no. 4, pp. 2980–2990, July 2019.

[23] S. Golshannavaz, S. Afsharnia, and F. Aminifar, "Smart distribution grid: Optimal day-ahead scheduling with reconfigurable topology," *IEEE Transactions on Smart Grid*, vol. 5, no. 5, pp. 2402–2411, 2014.

[24] H. M. A. Ahmed and M. M. A. Salama, "Energy management of ac–dc hybrid distribution systems considering network reconfiguration," *IEEE Transactions on Power Systems*, vol. 34, no. 6, pp. 4583–4594, 2019.

[25] M. Alhazmi, P. Dehghanian, S. Wang, and B. Shinde, "Power grid optimal topology control considering correlations of system uncertainties," *IEEE Transactions on Industry Applications*, vol. 55, no. 6, pp. 5594–5604, 2019.

[26] X. Qiao, Y. Luo, J. Xiao, Y. Li, L. Jiang, X. Shao, J. Xu, Y. Tan, and Y. Cao, "Optimal scheduling of distribution network incorporating topology reconfiguration, bes and load response: A milp model," *CSEE Journal of Power and Energy Systems*, pp. 1–12, 2020.

[27] M. Hotz and W. Utschick, "A hybrid transmission grid architecture enabling efficient optimal power flow," *IEEE Transactions on Power Systems*, vol. 31, no. 6, pp. 4504–4516, 2016.

[28] S. R. Salkuti, "Congestion management using optimal transmission switching," *IEEE Systems Journal*, vol. 12, no. 4, pp. 3555–3564, 2018.

[29] X. Li, A. S Korad, and P. Balasubramanian, "Sensitivity factors based transmission network topology control for violation relief," *IET Generation, Transmission Distribution*, vol. 14, no. 17, pp. 3539–3547, 2020.

[30] C. Lee, C. Liu, S. Mehrotra, and Z. Bie, "Robust distribution network reconfiguration," *IEEE Transactions on Smart Grid*, vol. 6, no. 2, pp. 836–842, 2015.

[31] R. A. Jabr, R. Singh, and B. C. Pal, "Minimum loss network reconfiguration using mixed-integer convex programming," *IEEE Transactions on Power Systems*, vol. 27, no. 2, pp. 1106–1115, 2012.

[32] Q. Peng, Y. Tang, and S. H. Low, "Feeder reconfiguration in distribution networks based on convex relaxation of opf," *IEEE Transactions on Power Systems*, vol. 30, no. 4, pp. 1793–1804, 2015.

[33] M. Khanabadi, H. Ghasemi, and M. Doostizadeh, "Optimal transmission switching considering voltage security and n-1 contingency analysis," *IEEE Transactions on Power Systems*, vol. 28, no. 1, pp. 542–550, 2013.

[34] Y. Yang, S. Zhang, W. Pei, J. Sun, and Y. Lu, "Network reconfiguration and operation optimisation of distribution system with flexible dc device," *The Journal of Engineering*, vol. 2019, no. 16, pp. 2401–2404, 2019.

[35] Y. Liu, J. Li, and L. Wu, "Coordinated optimal network reconfiguration and voltage regulator/der control for unbalanced distribution systems," *IEEE Transactions on Smart Grid*, vol. 10, no. 3, pp. 2912–2922, 2019.

[36] M. N. Abdul Rahim, H. Mokhlis, A. H. A. Bakar, M. T. Rahman, O. Badran, and N. N. Mansor, "Protection coordination toward optimal network reconfiguration and dg sizing," *IEEE Access*, vol. 7, pp. 163 700–163 718, 2019.

[37] Z. Yin, X. Ji, Y. Zhang, Q. Liu, and X. Bai, "Data-driven approach for real-time distribution network reconfiguration," *IET Generation, Transmission Distribution*, vol. 14, no. 13, pp. 2450–2463, 2020.

[38] W. E. Brown and E. Moreno-Centeno, "Transmission-line switching for load shed prevention via an accelerated linear programming approximation of ac power flows," *IEEE Transactions on Power Systems*, vol. 35, no. 4, pp. 2575–2585, 2020.

[39] K. W. Hedman, S. S. Oren, and R. P. O'Neill, "A review of transmission switching and network topology optimization," in *2011 IEEE Power and Energy Society General Meeting*, July 2011, pp. 1–7.

[40] K. W. Hedman, R. P. O'Neill, E. B. Fisher, and S. S. Oren, "Optimal transmission switching—sensitivity analysis and extensions," *IEEE Transactions on Power Systems*, vol. 23, no. 3, pp. 1469–1479, Aug 2008.

[41] B. Kocuk, S. S. Dey, and X. A. Sun, "New formulation and strong misocp relaxations for ac optimal transmission switching problem," *IEEE Transactions on Power Systems*, vol. 32, no. 6, pp. 4161–4170, Nov 2017.

[42] A. Gholami and X. A. Sun, "Towards resilient operation of multi-microgrids: An misocp-based frequency-constrained approach," *IEEE Transactions on Control of Network Systems*, vol. 6, no. 3, pp. 925–936, Sep. 2019.

[43] J. Dave, H. Ergun, T. An, J. Lu, and D. Van Hertem, "Tnep of meshed hvdc grids: 'ac', 'dc' and convex formulations," *IET Generation, Transmission Distribution*, vol. 13, no. 24, pp. 5523–5532, 2019.

[44] T. Altun, R. Madani, A. P. Yadav, A. Nasir, and A. Davoudi, "Optimal reconfiguration of dc networks," *IEEE Transactions on Power Systems*, pp. 1–1, 2020.

[45] J. Cao, W. Du, and H. F. Wang, "An improved corrective security constrained opf for meshed ac/dc grids with multi-terminal vsc-hvdc," *IEEE Transactions on Power Systems*, vol. 31, no. 1, pp. 485–495, 2016.

[46] K. W. Hedman, R. P. O'Neill, E. B. Fisher, and S. S. Oren, "Optimal transmission switching with contingency analysis," *IEEE Transactions on Power Systems*, vol. 24, no. 3, pp. 1577–1586, Aug 2009.

[47] S. Binato, M. V. F. Pereira, and S. Granville, "A new benders decomposition approach to solve power transmission network design problems," *IEEE Transactions on Power Systems*, vol. 16, no. 2, pp. 235–240, 2001.

[48] F. Zohrizadeh, M. Kheirandishfard, E. Q. Jnr, and R. Madani, "Penalized parabolic relaxation for optimal power flow problem," in *2018 IEEE Conference on Decision and Control (CDC)*, Dec 2018, pp. 1616–1623.

[49] R. Madani, M. Kheirandishfard, J. Lavaei, and A. Atamturk, "Penalized semidefinite programming for quadratically-constrained quadratic optimization," 2020.

[50] T. K. Vrana, Y. Yang, D. Jovcic, S. Dennetière, J. Jardini, and H. Saad, "The cigre b4 dc grid test system," *Electra*, vol. 270, no. 1, pp. 10–19, 2013.

[51] M. Grant and S. Boyd, "CVX: Matlab software for disciplined convex programming, version 2.1," http://cvxr.com/cvx, Mar. 2014.

[52] L. Gurobi Optimization, "Gurobi optimizer reference manual," 2018. [Online]. Available: http://www.gurobi.com

[53] X. Li, Z. Yuan, J. Fu, Y. Wang, T. Liu, and Z. Zhu, "Nanao multi-terminal vsc-hvdc project for integrating large-scale wind generation," in *2014 IEEE PES General Meeting— Conference & Exposition*. IEEE, 2014, pp. 1–5.

[54] D. Ingemansson, J. Wheeler, N. MacLeod, F. Gallon, and O. Ruiton, "The south-west scheme: a new hvac and hvdc transmission system in sweden," 2012.

[55] T. Nakajima and S. Irokawa, "A control system for hvdc transmission by voltage sourced converters," in *1999 IEEE Power Engineering Society Summer Meeting. Conference Proceedings (Cat. No. 99CH36364)*, vol. 2. IEEE, 1999, pp. 1113–1119.

[56] G. Tang, Z. He, H. Pang, X. Huang, and X.-p. Zhang, "Basic topology and key devices of the five-terminal dc grid," *CSEE Journal of Power and Energy Systems*, vol. 1, no. 2, pp. 22–35, 2015.

[57] J. Binkai and W. Zhixin, "The key technologies of vsc-mtdc and its application in china," *Renewable and Sustainable Energy Reviews*, vol. 62, pp. 297–304, 2016.

Tuncay Altun received his B.Sc. and M.Sc. degrees in Electrical Engineering from the Yıldız Technical University, Istanbul, Turkey, in 2011 and 2014, respectively. He received his Ph.D. degree at the University of Texas at Arlington, TX, USA, in 2020. He was a Postdoctoral Research Associate with the Department of Electrical Engineering at the University of Texas at Arlington, TX, USA. His research interests include optimization and control for power systems applications, renewable/sustainable energy systems, microgrids, and HVDC transmission.

Ramtin Madani received the Ph.D. degree in electrical engineering from Columbia University, New York, NY, USA, in 2015. He was a Postdoctoral Scholar with the Department of Industrial Engineering and Operations Research at University of California, Berkeley in 2016. He is an Assistant Professor with the Department of Electrical Engineering Department, University of Texas at Arlington, Arlington, TX, USA.

Ali Davoudi (S'04-M'11-SM'15) received the Ph.D. degree in electrical and computer engineering from the University of Illinois Urbana–Champaign, IL, USA, in 2010. He is currently a Professor with the Electrical Engineering Department, The University of Texas at Arlington, Arlington, TX, USA. He is an Associate Editor of the IEEE TRANSACTIONS ON POWER ELECTRONICS, and an Editor of the IEEE TRANSACTIONS ON ENERGY CONVERSION and the IEEE POWER ENGINEERING LETTERS. His research interests are various aspects of analysis and control of power electronics systems.